Assessment of the Vertical Accuracy of Satellite-Based Glacier Monitoring. The Rutor Glacier in Italy

Assessment of the Vertical Accuracy of Satellite-Based Glacier Monitoring. The Rutor Glacier in Italy

Myrta Maria Macelloni[1][0000-0002-2940-7977], Alberto Cina[1][0000-0003-4240-7987], Fabio Giulio Tonolo[2] [0000-0001-5783-0951] and Umberto Morra di Cella [3] [0000-0003-4250-9705]

[1] DIATI, Department of Environment, Land and Infrastructure Engineering, Politecnico di Torino, Corso Duca degli Abruzzi 24, 10129, Torino, Italy

[2] DAD – Department of Architecture and Design, Politecnico di Torino, Viale Pier Andrea Mattioli 39, 10125 Torino, Italy

[3] Environmental Protection Agency of Valle d'Aosta, Climate Change Unit, Loc. Grande Charrière, 48, 11020 Saint-Christophe (AO), Italy

myrta.macelloni@polito.it

Abstract. Periodical monitoring of glacier extent and volume changes is a fundamental tool, considering the relevant changes and volume losses glaciers have been undergoing in recent years. The climatological changes leading to increasing hazards and related risks in alpine areas require complex and updated 3D models. Specifically, mountain environments are characterised by complex orography and limited accessibility and often require risky and expensive in situ campaigns. The presented case stay is the Rutor Glacier (Aosta Valley, Italy), monitored and studied in a multidisciplinary framework by the Glacier Lab of the Politecnico di Torino and the Aosta Valley Environmental Agency (ARPA VDA). Different remote sensing platforms are being used to carry out an annual survey to generate detailed 3D models enabling the estimation of the mass balance, focusing on the 3D positional accuracy of the metric products. A very high-resolution Pleiades satellite image stereo pair acquired in September 2022 and a photogrammetric airborne survey carried out in the same month enable the comparison of 3D models based on different techniques and therefore characterised by different accuracies. In-depth analyses have been carried out to verify the suitability of satellite remote sensing for glacier monitoring, considering that a satellite-based approach would enable continuous monitoring over wide areas, including Alpine regions with limited access. The analyses are aimed at validating the 3D products by means of comparison with more accurate reference data as well as at evaluating the possibility of adopting synergistic multiscale approaches, exploiting satellite and aerial platforms.

Keywords: Satellite, Glaciers, Aerial, Photogrammetry, Vertical accuracy, 3D models

1 Introduction

The Department of Environment, Land and Infrastructure Engineering (DIATI) at Politecnico di Torino thanks to the Italian Ministry for Education and Research (MIUR), Dipartimento di Eccellenza funded the CC-LAB, a multidisciplinary laboratory for the climate changes. The activities of the Glacier Lab are mainly focus on the evolution of the glacier and periglacial areas under the effects of climate change with a multidisciplinary approach. Under this project, several glaciers were monitored during the last years in collaboration with geomatic, hydraulic and geophysics research groups of Politecnico di Torino to understands the dynamics and vulnerabilities of these complex systems.

Since 2020, in collaboration with the Environmental Protection Agency of Aosta Valley (ARPA VdA) the Rutor glacier was monitored by yearly monitoring campaigns, aerial photogrammetric surveys and very high resolution satellite images.

In this framework, remote sensing techniques are valid tools to monitor the cryosphere often used in the last 20 years (Paul et al, 2007) both to monitor water kinematics and dynamics (Fieber et al., 2008) and glacier retreat (Prinz et al., 2018, Giulio Tonolo, F. et al, 2020).

Satellite glacier images are usually used to study and monitor ice masses, especially those difficult to reach that necessitate recurring analysis (Otosaka et al., 2023), but their use in these areas is often challenging and could lead to inaccurate estimates in glacial mass balances (Zhang et al., 2023).

Starting from a set of high-resolution aerial and Satellite photogrammetric images acquired a few days apart, the main goal of the research is to evaluate the positional accuracies of the related added-value cartographic products (orthoimagery and Digital Surface Models - DSMs). In particular, the accuracy of the 3D satellite models is estimated exploiting both independent Check Points (CP) and DSMs of known accuracy and precision as reference dataset. Following this approach, it is possible to compare two DSMs of the same area generated in different periods and from different remote sensing techniques to appreciate the statistical significance of the altimetric and volumetric variations.

2 Materials and Methods

2.1 Case study

The Rutor Glacier is located in the north-western part of Italy, above La Thuile, at the border between Italy and France. It extends from 2540 m asl to 3486 m asl, and with its area of 7.9 km^2, is the third largest Aosta Valley glacier. The glacier has a gentle slope and is almost divided into two parts by the “Vedette du Rutor”, ending with three different tongues into a periglacial area of around 4 km2 characterised by lakes and moraines.

The Rutor glacier is retreating since Holocene maximum in 1820 when the extension was 12 km^2 (Villa et al., 2007) and has already lost 34% of its extent (Corte et al, 2023).

The projections (Intergovernmental Panel on Climate Change, Representation Concentration Pathway 8.5° C, IPCC RPC 8.5) of the climate scenarios estimate that the glacier will retreat up to 1.5 km in 2100 (Strigaro et al., 2016).

The continuous retreat strongly modifies the environment and the morphology and the hydrological system of the area and reduces the total water volume stored in the glacier. More specifically, the dynamics of the proglacial environment of the Rutor glacier created different moraines and lakes and sediment transport (Vergnano et al., 2023).

2.2 Reference data

Aerial orthoimagery (Ground Sample Distance – GSD of 0.10 m, resampled to 0.5 m for these analyses) and DSMs (GSD of 0.5 m) based of the aerial photogrammetric flight carried out on 13th September 2022 were extracted from the 3D point cloud and used as reference dataset to validate the satellites products. These products are based on visible imagery acquired with a Phase One camera onboard an ultralight aircraft and were processed in Agisoft Metashape v. 1.8.3 (Metashape, 2023). The flight altitude was about 974 m and the ground resolution of 7.45 cm/pix and scale of 1:20 000.
The 628 images of the 2022 model were elaborated with 9 Ground Control Points (GCPs) and 6 Check Points (CPs), i.e. artificial plastered markers positioned and measured with Global Navigation Satellite System (GNSS) receivers (Real time Kinematic - RTK mode) during ad-hoc field campaign. The reference system used is the RDN 2008 - EPSGS 6707. A summary of the different data considered in this work is reported in Table 1.

Table 1. Reference data

Product	Data	GSD
Aerial flight	13th September 2022	0.1 m (resampled to 0.5 m)
Satellite acquisition	11th September 2022	0.72 m (resampled to 0.5 m by the data provider)

A very high resolution (VHR) satellite stereo pair acquired from the Pleaides 1-A platform on 11th September 2022 at 10:23 was also processed (mean off-nadir angle of 23° over an area of 211.873 km^2 between Italy and France). The imagery includes visible (VIS) and near-infrared (NIR) information and is characterized by an actual GSD of 0.72 m for the panchromatic band and a 2.8 m for the multispectral ones.

The coverage of both aerial and Satellite acquisitions is shown in Figure 1.

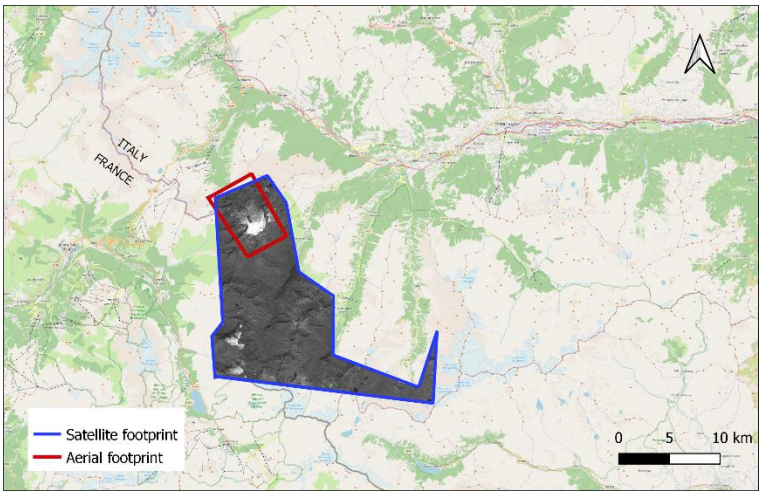

Fig. 1. Aerial (red) and Satellite (blu) coverage. Pléiades © CNES 2022 and AIRBUS DS

2.3 Data processing

The satellite stereo pair was processed with CATALYST Professional Version 2223.0.1 (Catalyst, 2023) using the Rational Function Model (RFM or RPC, Rational Polynomial Coefficients) non parametric approach. The panchromatic and multispectral images were preliminarily pansharpened to obtain high resolution multispectral images characterized by the spatial resolution of the panchromatic band.

Thanks to the fact that the reference aerial products (orthophoto and DSM) were acquired only two days after the satellite acquisition, an automatic identification of stereo GCPs, CPs and Tie Points (TPs) was possible (due to the limited changes among the acquisitions). All the points automatically identified were manually checked and refined. After the image orientation phase and the generation of the epipolar pair, the DSM was extracted and two orthophotos were generated.

The knowledge of the accuracy and precision of a DSM is critical information when comparing two DSMs of the same area related to different time periods. More specifically, the metadata are mandatory to appreciate the statistical significance of elevation changes within a given probability threshold. The threshold value above which elevation differences are statistically meaningful is referred to as the Limit of Detection (LoD). Once the LoD is known, it is possible to apply the error propagation theory to determine the confidence intervals of the height variations of the glacial mass, mainly due to ice melting or the corresponding volume variations between two different periods. We can determine the LoD of a DSM by comparison with independent reference products, generally following two alternative approaches:

- Calculation of 3D residuals on a few CPs measured with GNSS RTK.
- Comparison (pixel by pixel) against a reference DSM in areas considered stable, i.e.

Difference of DSMs (DoD) approach, focusing on stable areas in the periglacial zone and exploiting aerial surveys carried out in previous years (which are not the focus of this manuscript) (Azmoon et al, 2022). In our case, given the almost simultaneous aerial and satellite acquisitions, the entire area covered by the photogrammetric flight can be considered unchanged.

Both paths have advantages and limitations that are summarised in the following.

CPs can be measured with topographic techniques with an horizontal precision of 1.5-2 cm and a vertical precision of 2-3 cm. As far as the aerial survey is concerned, CPs can be considered an independent reference since they are unrelated to the photogrammetric process (the CP 3D accuracy is about 1/3 of the average aerial image GSD). However, CP numerosity is generally limited (6 in the specific case) since they need to be measured in the field and considering the accessibility constraints of a glacier environment.

The identification of control points on the imagery is often carried out manually with single pixel accuracy. Automatic sub-pixel accuracy is theoretically feasible using coded markers, but the operational constraints in the field make this approach mostly unusable in a glacier environment.

The second approach to determine the LoD is based on a statistical comparison with a DSM of known accuracy taken as reference. Being a pixel-by-pixel approach, the main advantage is that statistics are based on a very large number of points, but stable areas (without changes between the two datasets) must be defined to ensure that elevation differences are only due to measurement errors. It has to be highlighted that, even outside the glacier area subject to movements and melting, several phenomena may lead to variations, like instability processes, snow coverage, fluvial dynamics phenomena, water bodies, etc. Such areas induce errors in the image correlation phase leading to outliers in the DoD values that, if not properly filtered, severely impact on the statistics metrics.

In accordance to established testing practices in photogrammetry and topography, a maximum of 5% of the extreme values representing the tails of the DoD distribution have been excluded. Statistical analyses are carried out on this 95% sample, evaluating:

- Median over the entire sample, "robust" operator not influenced by the presence of gross errors;
- Mean and standard deviation of the DoD on the entire sample;
- Mean and standard deviation of the DoD on the 95% sample;
- Pearson indices based on mean and kurtosis on the 95% sample (their values are close to zero if the distribution is normal).

Being one of the goals to assess the possibility of using only satellite imagery for glacier monitoring (especially when no aerial reference data is available), a detailed sensitive analysis on GCP spatial configuration and numerosity has also been carried out. A variable set of GCPs was evaluated, ranging from no GCPs (i.e. direct georeferencing approach) to 10 GCPs, with at least 5 CPs to evaluate the impact of the GCP configurations on the 3D positional accuracy.

Both approaches were followed to determine the LoD of DSMs generated from:

- Aerial photogrammetry - September 2022 (not the focus of this manuscript): 6 CP and DoD with respect to the 2021 aerial dataset
- Satellite photogrammetry - September 2022: at least 5 CP and DoD with respect to the 2022 aerial dataset

For the assessment of the LoD of the satellite-based DSM, considering the one day difference between aerial and satellite acquisition dates, the DoD was carried out over the entire comparison area (as shown in Figure 2).

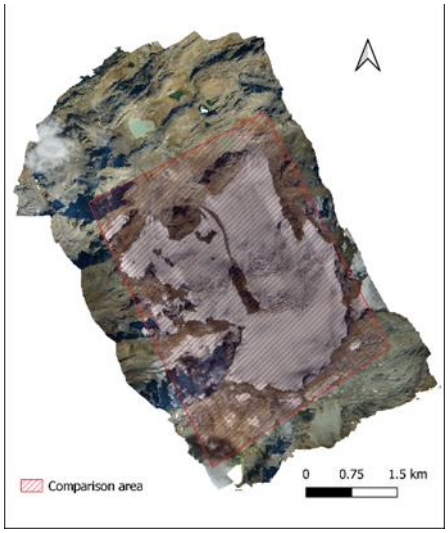

Fig. 2. Area considered for DoD on aerial orthophoto

3 Results

Concerning the evaluation of horizontal and vertical accuracy of the satellite based products using CP residuals, different configurations of GCPs (Table 2 and Figure 3) were tested when processing the satellite stereo-image.
The RMSEs on their CPs are reported in Table 3.

Table 2. Satellite RMSEs of different GCPs configurations

N GCPs	N CPs	GCPs ID	RMSE CP XY [m]	RMSE CP Z [m]
0	22	/	9.105	1.239
1	21	35	0.253	1.171
2	20	35,60	0.340	0.796
3	19	35,40,60	0.284	0.3650
5	13	35,39,40,60,61	0.140	0.651
10	8	all	0.147	0.760

It is clear from the results of Table 3 how the use of even just one GCP can eliminate horizontal and vertical systematic errors. Excellent results on the residuals calculated on the CPs are already obtained with only 3 GCPs. (see Table 4)

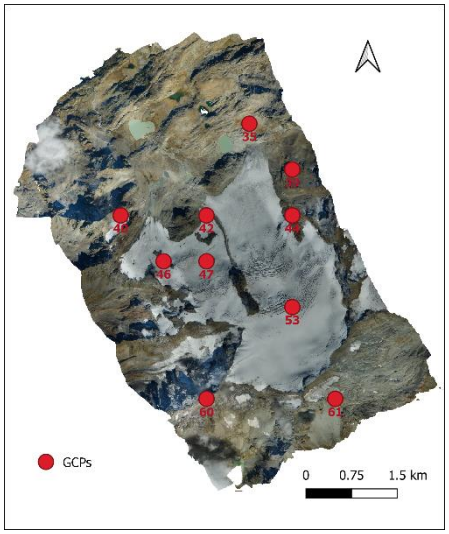

Fig. 3. Complete GCPs dataset spatial distribution and related ID

As already detailed, the satellite DSM is compared to the 2022 aerial DSM. Once the tails of the DoD distribution with significance level 5% are removed, the standard deviation of the altimetric differences is 56.8 cm (Fig. 4 and Table 4).
The trend of the deviations is shown in Figure 4 and Table 4, the cumulative frequency diagrams present the values of the height deviations in the abscissa and the frequencies between 0 and 1 in the ordinate.

To assume the accuracy of the satellite DSM (10 GCPs configurations), we can consider:

$$\sigma^2_{DSMaerial} + \sigma^2_{DSMsatellite} = (56.8)^2\ cm^2 \quad (1)$$

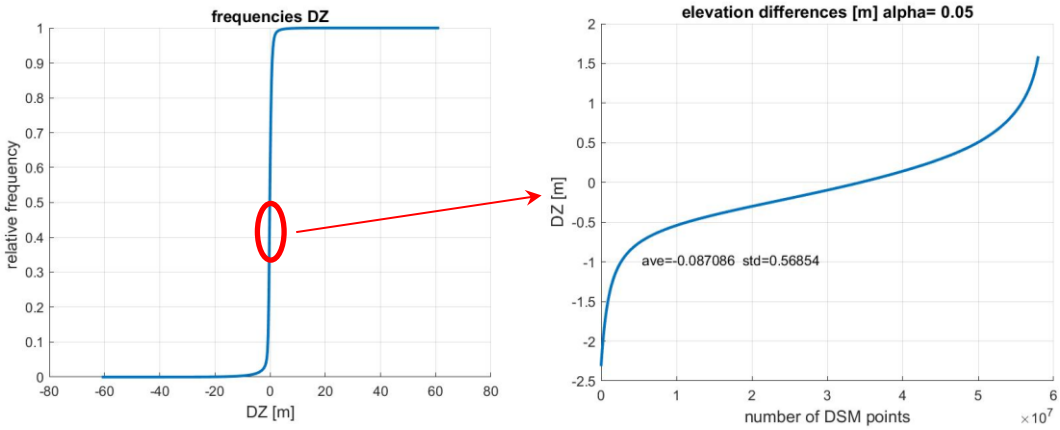

Fig. 4. Aerial 2022 - satellite2022 - alpha 5% 10GCPs

In the case of DSM by aerial photogrammetry, the accuracy was estimated from vertical residuals on 7 CPs with an RMS of 7.3 cm (Table 3). Independent analyses, not covered in this work, were made by comparing the DSMs of the stable areas of the 2022 photogrammetric model with that of the previous year. The results substantially confirm the accuracy obtained from the CP analysis. From the error propagation law, it is then possible to obtain the standard deviation of the Satellite DSM, knowing the standard deviation of the reference aerial DSM (2).

$$\sigma^2_{DSM\ satellite}=\sqrt{56.8^2-7.3^2}=\pm 56.3\ cm \quad (2)$$

As far as the analysis on the CPs is concerned, the root mean square errors (RMSE) of the different models on the CPs is reported in Table 3.

Table 3. CP RMSEs

Product	RMSE CP XY [m]	RMSE CP Z [m]
Aerial 2022	0.115	0. 073
Satellite 2022 (10 GCPs)	0.147	0.760

Based on the CPs, we then calculate the LoD of the differences between the DSMs (Figure 5) to assess the significance threshold:

$$\sigma^2_{DSM\ aerial\ -\ satellite}=\sqrt{7.3^2+76.0^2}=\pm 76.3\ cm \quad (3)$$

The two approaches lead to comparable LoD, which was used to classify the DoD, with the advantages and disadvantages highlighted in the previous section.

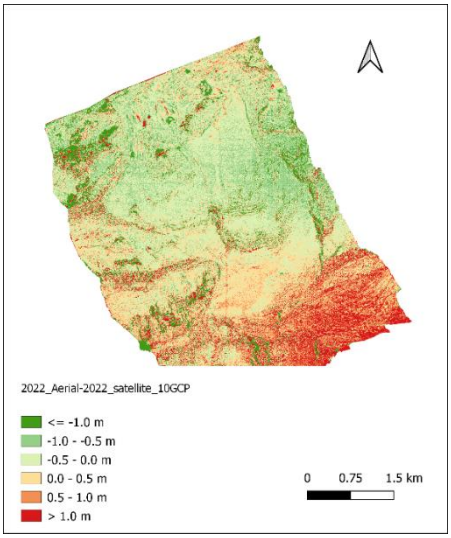

Fig. 5. DoD: Aerial 2022 – Satellite 2022

Additionally, to assess the accuracy of the different GCP configurations, using the procedure described above on the DoD area the statistics values are computed (Table 4 and Figure 6).

Table 4. Statistical analysis of differences between DSMs according to different configurations

	NO GCP	1 GCPs	2 GCPs	3 GCPs	5 GCPs	10 GCPs
% outlier > 10 m	6.930	0.351	0.450	1.681	0.405	0.410
Median [m]	2.581	1.147	0.595	0.626	0.13	-0.118
Mean [m]	1.997	1.071	0.591	0.792	0.0953	-0.156
Average without tails (5%) [m]	2.230	1.142	0.644	0.817	0.168	-0.087
Standard deviation without tails (5%) [m]	3.777	0.543	0.805	1.414	0.575	0.568
Skewness- Fisher range (without tails 5%)	-0.957	-0.223	0.142	0.661	-0.095	-0.068
Kurtosis- Fisher gamma 2 (no tails 5%)	1.798	0.921	0.413	3.035	1.115	1.022

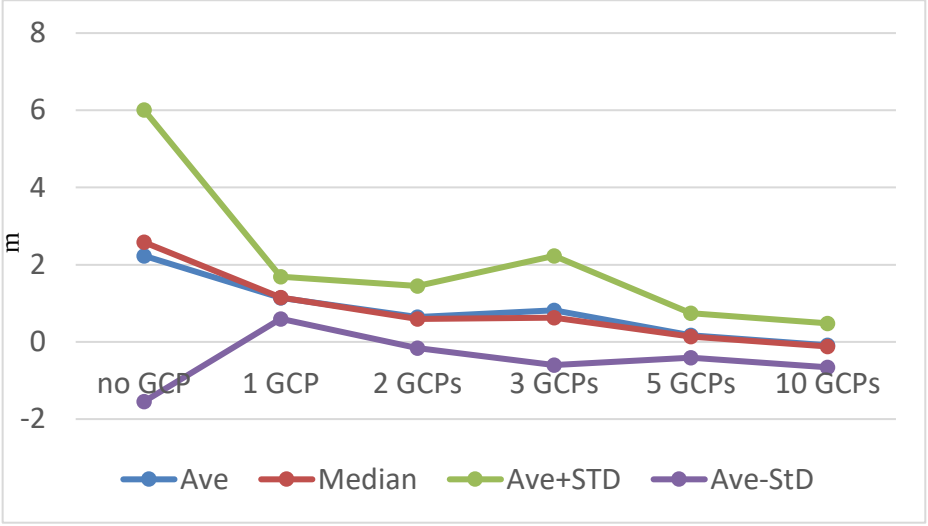

Fig. 6. DoD statistic metrics vs GCPs configurations

4 Discussion

As detailed in the Methods and Results sections, the assessment of the vertical precision of a DSM can be based on two approaches, exploiting as references

- a (generally) limited number of CPs;
- a DSM of higher accuracy and with a dataset population of (generally) dozens of millions.

In the latter case, it is crucial to exclude outliers that may originate where correlation fails. Generally, this happens on water bodies areas due to homogeneous patterns (e.g. lakes) or to variability among different frames in case of runoff. Analyzing the percentages of outliers above a threshold of 10 m for this case study, it can be noted that outliers are less than 2% on a correctly georeferenced DSM. We then cautiously exclude 5% of the tails of the DoD distribution, according to usual cartographic validation approaches.

It should be noted that statistics calculated on very large samples or samples of only a few units do not have the same reliability. The preliminary conditions for the application of a parametric statistic are that observations and errors are independent of each other and normally distributed. Small samples may not meet the assumptions of normal distribution. An alternative approach is to still use parametric tests relying on their robustness. However, the procedure applies to large samples and is generally not recommended (Krebs, 1999).

The hypothesis of Normal distribution can be verified by checking the skewness and kurtosis indices. The values of skewness and kurtosis of an experimental distribution, shown in Table 4 are given by Fisher's γ and γ_2 indices, respectively:

$$\gamma = \frac{m_3}{\frac{3}{m_2^2}}, \gamma_2 = \frac{m_4}{m_2^2} \quad (4)$$

with m2, m3 and m4 moments of the second, third and fourth order, respectively. It is shown by the Central Limit Theorem that in a distribution of sample averages the measures of skewness and kurtosis tend to zero as sample size increases. In a normal distribution the Fisher indices have zero value. We can check with a two-sided test whether:

- the skewness index is non-zero - null hypothesis H_0: $\gamma_1=0$ and alternative hypothesis H_0: $\gamma_1\neq0$
- the kurtosis index is different from zero-null hypothesis H_0: $\gamma_2=0$ and alternative hypothesis H_0: $\gamma_2\neq0$ using the standardized variables for skewness Z_{Skw} and kurtosis indices Z_{Kurt}:

$$Z_{Skw} = \frac{\gamma-0}{\sigma_1}, \sigma_1 = \sqrt{\frac{6}{n}}, Z_{Kurt} = \frac{\gamma2-0}{\sigma_2}, \sigma_2 = \sqrt{\frac{24}{n}} \quad (5)$$

on n sample size.

Table 4 shows that, normalizing the Fisher indices, the probability on both null hypotheses of skewness and kurtosis is practically equal to 1 on the 95% sample. This implies that the mean and standard deviation parameters of the DoD between the satellite and aerial DSM are well representative of a normal distribution. With this assumption we can say that the most representative value of LoD of the satellite DSM is 57 cm (68% probability interval: the value is double at 95% probability interval). This value is coherent with the nominal spatial resolution of the satellite images.

Concerning the use of GCPs for the orientation of the satellite stereo pair, it has to be remarked that – despite GCPs are crucial for the datum definition and for the final positional accuracy - there are several operational constraints related to GCP materialisation and measurement in glacial or periglacial areas. This operation should therefore be limited as much as possible. The statistical analysis of the result of different configurations of GCPs is aimed at identifying the minimum and optimal number of GCPs to be used.

Table 4 and Figure 6 show the DoD statistic metrics with different configurations of GCPs. A direct georeferencing approach (i.e. no GCP) is possible (with a vertical accuracy of few meters), it is recommended to use at least 1 GCP to correct systematic effects. Increasing the number of GCPs leads to a significant improvement up to 5 GCPs.

5 Conclusions

In glaciological activities, the measurement of ground variations is used for the analysis of melting phenomena and related consequences. Such analyses are increasingly approached with photogrammetric surveys for the generation of 3D models: therefore, it

is crucial to know their horizontal and vertical precision to statistically assess whether multitemporal elevation differences can be considered statistically meaningful. Among the different platforms that can be used for photogrammetric surveys, satellites enable the acquisition of large areas (covering several glaciers) also if hardly accessible on the ground.

The analyses carried out for this research focused on very high resolution satellite stereo pairs. The results show that 5 GCPs, homogeneously distributed over the stereo pair footprint, enable to achieve sub-meter vertical accuracy (i.e. same order of magnitude of the image GSD) and imply a conservative but sustainable number of ground measurement operations. However, GCPs can be derived from photogrammetric products at larger nominal map scale (and therefore accuracy) when available.

The satellite DSM validation was carried out by evaluating elevation differences with respect to CPs and a reference aerial DSM. A LoD (at 68%, 1 standard deviation) of 76 cm and 57 cm respectively was estimated. According to the discussion section, the value of 57 cm seems a reasonable LoD since it is based on a sample of 60 M points.

The robustness of future multi-temporal analyses can be measured using parametric statistics, after verifying the hypothesis of DoD normal distribution based on skewness and kurtosis indices. This hypothesis is met by conservatively considering 95 percent of the DoD population, excluding the maximum and minimum values of the tails of the DoD distribution.

Funding

The Italian Ministry for Education and Research (MIUR), Dipartimento di Eccellenza, sui cambiamenti climatici, funded this research. (https://www.diati.polito.it/focus/dipartimento_di_eccellenza_sui_cambiamenti_climatici_2018_2022/laboratorio_multisito/cc_glacier_lab) and ARPA Valle d'Aosta. The Pléiades satellite images were provided by AIRBUS Defense & Space in the framework ISIS License EU V4 -DIN-PGO-2022-HN-GRAN PARADIS.

References

1. Paul, F., Kääb, A., Haeberli, W. (2007). Recent glacier changes in the Alps observed by Satellite: Consequences for future monitoring strategies. Global and Planetary Change, 56 1–2), 111–122. https://doi.org/10.1016/j.gloplacha.2006.07.007
2. Fieber, K. D., Mills, J. P., Miller, P. E., Clarke, L., Ireland, L., Fox, A. J. (2018). Rigorous 3D change determination in Antarctic Peninsula glaciers from stereo WorldView-2 and archival aerial imagery. Remote Sensing of Environment, 205, 18–31. https://doi.org/10.1016/j.rse.2017.10.042
3. Prinz, R., Heller, A., Ladner, M., Nicholson, L. I., & Kaser, G. (2018). Mapping the loss of Mt. Kenya's glaciers: An example of the challenges of satellite monitoring of very small glaciers. *Geosciences (Switzerland)*, *8*(5). https://doi.org/10.3390/geosciences8050174
4. Giulio Tonolo, F., Cina, A., Manzino, A., & Fronteddu, M. (2020). 3D GLACIER MAPPING by MEANS of SATELLITE STEREO IMAGES: The BELVEDERE GLACIER CASE STUDY in the ITALIAN ALPS. *International Archives of the Photogrammetry,*

Remote Sensing and Spatial Information Sciences - ISPRS Archives, *43*(B2), 1073–1079. https://doi.org/10.5194/isprs-archives-XLIII-B2-2020-1073-2020

5. Otosaka, I. N., Horwath, M., Mottram, R.; Nowicki, S. (2023). Mass Balances of the Antarctic and Greenland Ice Sheets Monitored from Space. In Surveys in Geophysics Springer Science and Business Media B.V. https://doi.org/10.1007/s10712-023-09795-8
6. Zhang, G., Bolch, T., Yao, T., Rounce, D. R., Chen, W., Veh, G., King, O., Allen, S. K., Wang, M., & Wang, W. (2023). Underestimated mass loss from lake-terminating glaciers in the greater Himalaya. *Nature Geoscience*, *16*(4), 333–338. https://doi.org/10.1038/s41561-023-01150-1
7. Villa, F., De Amicis, M., and Maggi, V. (2007), GIS analysis of Rutor Glacier (Aosta Valley, Italy) volume and terminus variations, Geogr. Fis. Din. Quat., 30, 87–95.
8. Corte, E., Ajmar, A., Camporeale, C., Cina, A., Coviello, V., Tonolo, F. G., Godio, A., Macelloni, M. M., Tamea, S; Vergnano, A. (preprint 2023.). Multitemporal characterisation of a proglacial system: a multidisciplinary approach. https://doi.org/10.5194/essd-2023-94
9. Strigaro, D., Moretti, M., Mattavelli, M., Frigerio, I., Amicis, M. D., and Maggi, V.: (2016) A GRASS GIS module to obtain an estimation of glacier behavior under climate change: A pilot study on Italian glacier, Comput. Geosci., 94, 68–76, https://doi.org/10.1016/j.cageo.2016.06.009.
10. Vergnano, A., Oggeri, C.,; Godio, A. (2023). Geophysical–geotechnical methodology for assessing the spatial distribution of glacio-lacustrine sediments: The case history of Lake Seracchi. Earth Surface Processes and Landforms,48(7), 1374–1397. https://doi.org/10.1002/esp.5555
11. *Agisoft Metashape: Agisoft Metashape*. (n.d.). Retrieved July 21, 2023, from https://www.agisoft.com/
12. Azmoon, B., Biniyaz, A., & Liu, Z. (2022). Use of High-Resolution Multi-Temporal DEM Data for Landslide Detection. *Geosciences (Switzerland)*, *12*(10). https://doi.org/10.3390/geosciences12100378
13. *CATALYST.Earth - Home*. (n.d.). Retrieved July 21, 2023, from https://catalyst.earth/
14. Krebs, C.J. 1999. Ecological Methodology, 2nd ed. Addison-Wesley Educational Publishers.